AD-A133 516 THEORETICAL AND EXPRRIMENTAL STUDIES OF THE ELECTRONIC STRUCTURE OF THE M..(U) INDIANA UNIV AT BLOOMINGTON DEPT OF CHEMISTRY M H CHISHOLM ET AL. 08 SEP 83 1/1

UNCLASSIFIED INDU/DC/TR-83/5-MC N00014-79-C-0044 F/G 7/4 NL

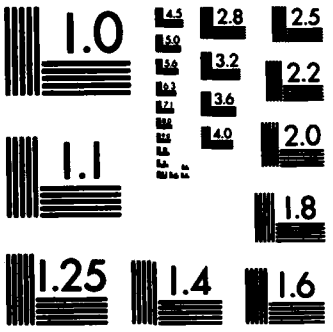

MICROCOPY RESOLUTION TEST CHART
NATIONAL BUREAU OF STANDARDS-1963-A

(12)

AD-A133 516

OFFICE OF NAVAL RESEARCH

Contract No. N00014-79-C-0044

Task No. NR 056-703

TECHNICAL REPORT NO. INDU/DC/TR-83/5-MC

THEORETICAL AND EXPERIMENTAL STUDIES OF THE ELECTRONIC STRUCTURE OF THE $Mo_3(\mu_3\text{-}O)(\mu_3\text{-}OR)(\mu\text{-}OR)_3(OR)_6$ TYPE OF TRIANGULO METAL ATOM CLUSTER COMPOUND

by

M.H. Chisholm, F.A. Cotton, Anne Fang and E.C. Kober

Prepared for Publication

in

Inorganic Chemistry

Department of Chemistry
Indiana University
Bloomington, IN 47405

September 8, 1983

SECURITY CLASSIFICATION OF THIS PAGE (When Data Entered)

REPORT DOCUMENTATION PAGE

READ INSTRUCTIONS BEFORE COMPLETING FORM

1. REPORT NUMBER: INDU/DC/TR-83/5-MC	2. GOVT ACCESSION NO.: AD-A133516
3. RECIPIENT'S CATALOG NUMBER:	
4. TITLE (and Subtitle): Theoretical and Experimental Studies of the Electronic Structure of the $Mo_3(\mu_3\text{-}O)(\mu_3\text{-}OR)(\mu\text{-}OR)_3(OR)_6$ Type of Triangulo Metal Atom Cluster Compound	5. TYPE OF REPORT & PERIOD COVERED: Technical Report 1983
	6. PERFORMING ORG. REPORT NUMBER: INDU/DC/TR-83/5-MC
7. AUTHOR(s): M.H. Chisholm, F.A. Cotton, A. Fang and E.C. Kober	8. CONTRACT OR GRANT NUMBER(s): N00014-79-C-0044
9. PERFORMING ORGANIZATION NAME AND ADDRESS: Department of Chemistry, Indiana University, Bloomington, IN 47405	10. PROGRAM ELEMENT, PROJECT, TASK AREA & WORK UNIT NUMBERS:
11. CONTROLLING OFFICE NAME AND ADDRESS: Office of Naval Research, Department of the Navy, Arlington, VA 22217	12. REPORT DATE: September 8, 1983
	13. NUMBER OF PAGES: 29
14. MONITORING AGENCY NAME & ADDRESS(if different from Controlling Office):	15. SECURITY CLASS. (of this report):
	15a. DECLASSIFICATION/DOWNGRADING SCHEDULE:

16. DISTRIBUTION STATEMENT (of this Report)

This document has been approved for public release and sale; its distribution is unlimited.

17. DISTRIBUTION STATEMENT (of the abstract entered in Block 20, if different from Report)

18. SUPPLEMENTARY NOTES

19. KEY WORDS (Continue on reverse side if necessary and identify by block number)

triangulo metal atom clusters, molybdenum, alkoxide, oxo, electronic structure, Fenske-Hall calculation, electrochemistry, UV-visible spectroscopy

20. ABSTRACT (Continue on reverse side if necessary and identify by block number)

The electronic structure of a $Mo_3(\mu_3\text{-}O)(\mu_3\text{-}OR)(\mu_2\text{-}OR)_3(OR)_6$ molecule with R = H, and C_{3v} symmetry, which serves as a model for real molecules in which R = $CH_2C(CH)_3$ or $CH(CH_3)_2$ has been calculated by the molecular orbital method of Hall and Fenske. The calculations have been performed not only on the entire molecule, but on the Mo_3^{12+}, $Mo_3O(OH)^{9+}$ and $Mo_3O(OH)_4^{6+}$ fragments

DD FORM 1 JAN 73 1473 EDITION OF 1 NOV 65 IS OBSOLETE
S/N 0102-014-6601

SECURITY CLASSIFICATION OF THIS PAGE (When Data Entered)

and the metal-metal bonding tracked through these successive stages by the "clusters in molecules" formalism. In the full molecule, the HOMO is an e orbital that carries most of the e-type M-M bonding, while the a_1-type is carried by two MO's, one of which is quite stable. The LUMO is also an e type orbital and the HOMO-LUMO gap is small (ca. 1.5 eV). It is predicted that the $Mo_3O(OR)_{10}$ molecules of this type will have readily accessible redox chemistry in which both oxidation and reduction steps might be slowed or irreversible judging by the character of the HOMO and LUMO of the $Mo_3O(OR)_{10}$ molecule. Experimental observations on $Mo_3O(ONe)_{10}$, Ne = $CH_2C(CH_3)_3$, are in harmony with this. In addition, the absorption spectrum of $Mo_3O(ONe)_{10}$ has been observed and an assignment based on the calculations in proposed.

Introduction

The group VI elements, molybdenum and tungsten, show a remarkable predilection to form equilateral triangular metal atom cluster compounds,[2] and such clusters are also formed by other early transition elements,[3] such as niobium.[4] Previous studies by Cotton and coworkers, in collaboration with colleagues in Haifa and Jerusalem, have provided experimental data as well as theoretical analysis[2,5] of compounds with the $[M_3(\mu_3\text{-}X)_2(O_2CR)_6L_3]$, $[M_3(\mu_3\text{-}X)(\mu_2\text{-}Y)_3L_9]$ and $[M_3(\mu_3\text{-}X)(O_2CR)_6L_3]$ type compounds. Theoretical work has also been done on related systems.[6,7]

In 1981, Chisholm and coworkers[8] reported the existence of yet another structural type, Fig. 1, of trinuclear molybdenum(IV) cluster compound. We have employed the compound $Mo_3O(ONe)_{10}$, where Ne represents the neopentyl group, $(CH_3)_3CCH_2$, to conduct experimental studies of this molecule and the ~~cation~~ anion $[Mo_3O(ONe)_{10}]^-$ bearing on the electronic structures of such species. We have also carried out a theoretical analysis of $Mo_3O(OH)_{10}$ as a model of this type of comound, employing the Fenske-Hall[9] method of calculation, to see how the bonding here would compare with that in the three types of cluster compounds previously treated, and to see if an understanding of the redox chemistry and absorption spectrum of this type of cluster could be achieved. The results are reported and discussed here.

Experimental and Computational Procedures

The Fenske-Hall calculations were carried out in a manner previously described in detail.[5-7] The structural parameters reported by Chisholm et al.[8] were idealized to C_{3v} symmetry and the OR groups were replaced by OH.

Standard experimental techniques for the manipulation of air- and water-sensitive materials were employed. The compound $Mo_3O(ONe)_{10}$ was prepared as previously described.[8] Electronic absorption spectra were obtained with a Hitachi 330 recording spectrophotmeter. Samples were run versus a solvent blank using matched 1 cm or 1 mm quartz cells. The cyclic voltammograms were obtained using a PAR 173 potentiostat, a PAR 175 programmer and a Houston 2000 XY recorder. A three-compartment cell was used with a platinum bead or gauze working electrode, a platinum wire auxiliary electrode and a Ag/AgCl pseudo-reference electrode. A 0.2 M solution of tetra-n-butyl ammonium hexafluorophosphate (TBAH) was employed as supporting electrolyte. No internal resistance compensation was used. Scan rates were 200 mV/sec. EPR measurements (X-band) were made on a Varian E-3 spectrophotometer.

Results and Discussion

Calculations. We shall first examine the theoretical picture of the bonding provided by the calculations and then analyze the experimental observations in the light of this description. The conceptual basis of the calculations, as before in our work on other trinuclear clusters,[5-7] is the "clusters in molecules" idea. The results for any given stage of ligation of the M_3 cluster are resolved into contributions from ligand orbitals and from MO's of the M_3 cluster (rather than individual atomic orbitals of the M atoms). In this way the existence and bonding characteristics of the M_3 cluster as a central entity surrounded by ligands are kept clearly at the center of attention.

To implement this "clusters in molecules" approach we begin, naturally, with a calculation of the MO's for the bare cluster, e.g., Mo_3^{12+} with an Mo-Mo distance of 2.529Å, in this case. Only the five $\underline{d}$ orbitals of each metal atom play any significant role in the bonding and these give rise to the set of ten MO's listed in Table I; for the bare cluster the symmetry is D_{3h} and the MO's are designated accordingly. This symmetry (and the notation) will change to C_{3v} as soon as ligands are added. It can be seen from Table I that the two most strongly bonding (and occupied) MO's are $1a_1'$ and $1e'$, which arise almost entirely as combinations of atomic $\underline{d}_{z^2}$ and $\underline{d}_{xz}$ orbitals, respectively. In general, the entire picture of the bare Mo_3^{12+} cluster is the same as that obtained before[5-7] at somewhat different Mo-Mo distances.

The MO's were calculated for each of the intermediate stages of ligation of the cluster, i.e., for $[Mo_3(\mu_3\text{-}O)(\mu_3\text{-}OH)]^{9+}$ and $[Mo_3(\mu_3\text{-}O)(\mu_3\text{-}OH)(\mu_2\text{-}OH)_3]^{6+}$, as well as for the final complete molecule, $[Mo_3(\mu_3\text{-}O)(\mu_3\text{-}OH)(\mu_2\text{-}OH)_3(OH)_6]$. The progressive spreading of the cluster MO's into the total electronic structure of the molecule as a whole can thus be followed step by step. We shall not report all these intermediate results in detail here, but look selectively at a few key aspects and then at the final result. More details are available from the authors on request.

At the left of Fig. 2 are shown the lowest five cluster MO's at the energies they have after interacting with μ_3-O and μ_3-OH. In the next column, moving towards the right, are the central MO's of the $Mo_3O(OH)^{9+}$ unit. Omitted are the $1a_1$ and $2a_1$ MO's which are O-H and oxygen $\underline{2s}$ orbitals of μ_3-OH and μ_3-O, respectively. Tie lines

between the first two columns show the principal ways in which the Mo_3^{12+} orbitals contribute to the $Mo_3O(OH)^{9+}$ MO's. The $3a_1$ and 2e orbitals are mainly responsible for Mo_3 to μ_3-OH bonding, while the $4a_1$ and 1e orbitals carry most of the Mo_3 to μ_3-O bonding. The metal-metal bonding is principally carried by the 3e and $5a_1$ orbitals which have 68% and 72% metal character, respectively. The $5a_1$ orbital is the HOMO.

With the addition of the three μ_2-OH ligands we get the array of orbitals shown in the next column of Fig. 2. Not shown are the $1a_1$, $2a_1$, 1e and $3a_1$ MO's that lie in the range -22.2 to -22.6 eV. The first three are essentially O-H bonding orbitals and $3a_1$ is essentially the 2s orbital of μ_3-O. All of the virtual orbitals now lie at energies above those shown and the HOMO is the 7e orbital. This is by far the major e-type contributor to metal-metal bonding. The a_1 component of metal-metal bonding is shared by the $7a_1$ and $6a_1$ MO's.

The calculation for the entire $Mo_3O(OH)_{10}$ molecule gave results that are shown, in part, at the right side of Fig. 2 and listed in Table II. Between -26.7 eV and -21.1 eV are all of the MO's that are principally O-H bonding in nature and made up mainly of oxygen 2s and hydrogen 1s atomic orbitals, and the 2s orbital of the μ_3-O atom, with essentially no metal orbital contribution. These are $1a_1$, $2a_1$, $3a_1$, $4a_1$, $5a_1$, 1e, 2e and 3e.

The molecular orbitals responsible for the Mo-O bonds and oxygen lone pairs are distributed through the energy range -10.7 to -1.4 eV, as can be seen in Table II. In most cases the provenance of these MO's in the O, OR and Mo_3 moieties is so mixed that no simple description of their bonding role is possible. Notable exceptions are the a_2 orbitals. The $1a_2$ orbital is a weakly bonding but mainly lone pair orbital on the μ_2-OH groups. It lies

mainly in the $Mo_3(\mu_2\text{-}O)_3$ plane. The $2a_2$ and $3a_2$ MO's are occupied by what are essnetially lone pairs on the terminal OH oxygen atoms.

We turn now to some of the orbitals that will be most pertinent to a discussion of the metal-to-metal bonding, the redox chemistry and the electronic absorption spectrum of the compound. These orbitals, shown in Fig. 3, are the 15e, 16e, $10a_1$ and $14a_1$ orbitals. To fully convey their spatial characteristics, each one is represented by contours in the Mo_3 plane and by a section perpendicular to this plane and including either two metal atoms (e orbitals) or a vertical mirror plane (a_1 orbitals).

Metal-to-metal bonding is somewhat distributed over two a_1 and several e type orbitals. The e component of M-M bonding receives its largest contribution from the HOMO, the 15e orbital, but significant contributions also come from the 10e and 8e orbitals. The a_1 component of M-M bonding is derived in part from the second-highest filled orbital, $14a_1$, but also, to an even greater extent from the $10a_1$ orbital. Both of these a_1 orbitals, but especially the $14a_1$ orbital, are also significantly involved in bonding of the Mo_3 cluster to the μ_3-O atom.

The LUMO, 16e, comes close to having a nodal plane coincident with the Mo_3 plane. This is because its parentage is largely in e" type orbitals of the bare Mo_3 cluster and these (in the D_{3h} symmetry of the bare Mo_3 cluster) have a rigorous nodal plane. Thus, while the HOMO is an e orbital of essentially σ Mo-Mo bonding type the LUMO is an e orbital of essentially π Mo-Mo bonding type. The LUMO, however, is markedly antibonding with respect to all of the Mo-(μ_3-O), Mo-(μ_3-OH) and Mo-(OH) bonds.

In Table III are presented the Mulliken populations of the canonical cluster orbitals at each stage of the process of ligating the cluster. It is seen that after an initial drop when the μ_3-O and μ_3-OH ligands are added, the la_1' and le' cluster orbitals continue to be well populated and thus they constitute a continuing and principal source of metal-metal bonding throughout. The average charge per metal atom in the neutral molecule is approximately +1, which is a reasonable value for metal atoms formally in oxidation state +4 and combined with relatively electronegative oxygen atoms.

Some Predictions. It is to be noted that the HOMO-LUMO gap is not large, ca. 1.5 eV. (1) This should mean that either oxidation or reduction, or both, should be chemically feasible processes for compounds of this class. For either process the resulting ion should have an electron in an e orbital. (2) The characters of both HOMO (15e) and LUMO (16e) are such that significant structural changes might be expected upon either oxidation or reduction. Thus, while these processes might be achievable at relatively low potentials, they might well be expected to lack reversibility. (3) Because of the low symmetry a considerable number of formally allowed one-electron transitions are to be expected. Some of these should be found in the visible region, and several might well be strong. We shall return to this question in more detail when the observed spectrum is discussed.

An Alternate, Qualitative View of the Metal-Metal Bonding. We first note that the structure (Fig. 1) we are dealing with can be constructed from three distorted MoO_6 octahedra fused along one common edge, and thus having two vertices (the μ_3-O and μ_3-OR groups) common to all three octahedra. If we neglect the distortions each metal may be said to use two d orbitals in Mo-O σ bonding (the e_g orbitals in an ideal octahedron) and then to have

three more d orbitals (the t_{2g} orbitals of an ideal octahedron) available to contain the two d electrons and to be employed in both Mo-Mo bonding and Mo-O π bonding. If we ignore the latter, as a first approximation, we may use the three sets of "t_{2g}" type d orbitals to construct molecular orbitals that can be used for metal-metal bonding.

In the spirit of the concept that the bonding or antibonding character of the resulting MO's will be proportional to the magnitudes of the overlaps (positive or negative, respectively) and with a few necessary but trivial coordinate transformations to obtain overlap expressions that are related to the types available in tables,[10] the relative energies of the resulting orbitals were estimated. We also used D_{3h} symmetry since a conjunction of ideal octahedra would yield this rather than the actual C_{3v} symmetry. In this way we get the following three-center MO's, which are listed in order of increasing energy (those of M-M antibonding character carry an asterisk):

$$a_1' \leq e' < e'' < a_1^* < e'^* \leq a_2'^*$$

This sequence of orbitals is in good agreement with those listed in Table I. In the order given above they correspond to the $1a_1'$, $1e'$, $1e''$, $1a_1''$, $3e'$ and $1a_2'$ orbitals of the Mo_3^{12+} cluster. The first three correspond crudely to the $14a_1$, 15e and 16e orbitals of the complete $Mo_3O(OH)_{10}$ molecule. Thus, even this very drastically simplified approach to the bonding suggests, correctly, that the metal-metal bonding is accomplished by six electrons occupying an a_1 + e pair of orbitals of bonding character and that the lowest empty MO of significant metal d orbital parentage (also bonding in the M-M sense) is also an e type orbital, but one of approximately π symmetry relative to the molecular plane.

There may be those who would question the value of the preceding exercise in drastically simplified bonding analysis. We believe it adds a sense of qualitative or intuitive reality that enhances confidence in the more quantitative results. We may now turn to some experimental results that ought to be in harmony with the theoretical picture just developed.

Electrochemistry. The electrochemical properties of $Mo_3O(ONe)_{10}$ were examined in both THF and CH_2Cl_2 solutions. In THF, two reductive waves were observed as is illustrated in Figure 4A. The first wave, with $E_{\frac{1}{2}} = -0.91V$, has a rather large peak separation of 180 mV indicating some irreversibility to the reduction process. With our experimental setup, reversible couples (such as ferrocene/ferrocenium) exhibited peak separations of 90-120 mV (versus the 60 mV anticipated) indicating that part of the large separation is due to uncompensated internal resistance.

Reductive coulometry at -1.2 V established that this first wave is a one-electron couple. A subsequent cyclic voltammogram was the same as the initial scan. This implies that the integrity of the complex is maintained during the reduction process. There is, in fact, evidence for fairly long term stability of the resulting anion. For one thing the reductive and (reverse) oxidative peak heights are equal. It was further shown that even after several hours, oxidative coulometry at 0.0 V regenerated the original species, as determine by electronic absorption spectroscopy.

It thus appears that while the first reduction process is a reversible one, it may be slow because of some energy barrier. According to the electronic structure calculations the electron must enter an orbital (16e) that has simultaneously metal-metal bonding character and metal-ligand

antibonding character; moreover, introduction of an electron into this e-type orbital should lead to distortion, according to the Jahn-Teller theorem. It might thus be that the equilibrium structure of the reduced species differs appreciably from that of the neutral molecule and that a significant barrier must be surmounted to pass from one nuclear configuration to the other.

The second reductive wave, with $E_{\frac{1}{2}} = -1.95$ V, shows a larger peak separation (250 mV) than the first. The similarity in peak heights suggest that it is also a one electron couple. The oxidative peak height appears to be smaller than that for reduction. Unfortunately, the proximity of this couple to the solvent limit of -2.5 V prevented us from further investigating the properties of the doubly reduced species. No oxidative waves were observed in THF out to the solvent limit of +1.0 V.

The electrochemical properties of $Mo_3O(ONe)_{10}$ in CH_2Cl_2 solution are somewhat different. The first reduction occurs at -1.33 V with a peak separation of 220 mV. The second reduction is not observed, apparently occurring beyond the solvent limit of -1.8 V. Moreover, in CH_2Cl_2 an oxidation wave is observed and this is shown in Figure 4B. The oxidative peak is at E = +0.88, and thereis a complete absence of a reductive component (even at 500 mV/sec), implying that the process is chemically irreversible. A reductive wave is observed to grow in at ~-0.5 V upon cycling through the oxidative wave, but the decomposition product that gives rise to this is not yet identified. Since oxidation should remove an electron from the 15e orbital which is strongly metal-metal bonding, it is reasonable that this might lead to enough disruption of the structure to make the oxidation an irreversible process.

EPR Spectra. The electrochemically generated $Mo_3O(ONe)_{10}^{1-}$ species in THF (0.2 M TBAH) exhibited an EPR signal at 77 K. The signal was centered at g = 2.047 and could be seen to be anisotropic. Hyperfine coupling to the $^{95,97}Mo$ nuclei (I = 5/2, 25.4%) was observed with $A \approx 2.4 \cdot 10^{-3}$ cm^{-1}. The EPR spectrum is being further studied and will be described in more detail in a future report.

Electronic Absorption Spectrum. The absorption spectrum for $Mo_3O(ONe)_{10}$ dissolved in hexane is shown in Figure 5, with the band positions and extinction coefficients summarized in Table IV. As can be seen, the relatively simple spectrum consists of two weak bands ($\varepsilon \sim 500$) in the visible region and two strong bands ($\varepsilon \sim 20{,}000$) in the UV. The green color of the complex is understandable in terms of this absorption spectrum.

To determine probable assignments for the observed absorption bands we shall consider the two higher filled orbitals, $14a_1$ and 15e and the four lowest virtual orbitals 16e, $4a_2$, 17e and $5a_2$. We first note that although the total symmetry of the molecule is C_{3v}, the Mo_3 core has D_{3h} symmetry and there is little mixing between orbitals of different D_{3h} symmetry types for the six orbitals of concern (see Table II). Transitions among them might then be effectively governed by the selection rules of a D_{3h} molecule. On this basis, only four of the possible eight orbital transitions are found to be allowed. These are listed in Table IV along with first order estimates of the transition energy, which are simply based on orbital energy differences.

Also included in Table V are qualitative estimates of the relative transition intensities, i.e., strong or weak. The basis for these intensity predictions is as follows. It is seen that the 15e and $5a_2$ orbitals have large contributions from the same d orbital type (d_{xz}), whereas the a_2

orbital contains an in-phase combination of the $\underline{d}_{xz}$ orbitals and the e orbital an out-of-phase combination. These two orbitals will then essentially differ from one another only in respect to a single symmetry plane: one orbital will be symmetric with respect to this plane while the other will be antisymmetric. Since transitions between orbitals which differ from one another simply by behavior with respect to a symmetry plane are strongly allowed (e.g., atomic $\underline{s} \longleftrightarrow \underline{p}$, $\underline{p} \longleftrightarrow \underline{d}$ etc. transitions), it is expected that the $15e \longrightarrow 5a_2$ should be strongly allowed. The same argument holds for the $14a_1 \longrightarrow 17e$ transition since both orbitals have heavy contributions from the $\underline{d}_{z^2}$ orbitals.

The remaining two transitions are seen to be between molecular orbitals which are built up of different types of metal $\underline{d}$ orbitals: $15e(\underline{d}_{xz}) \longrightarrow 16e(\underline{d}_{xy})$ and $15e(\underline{d}_{xz}) \longrightarrow 17e(\underline{d}_{z^2}, \underline{d}_{x^2-y^2})$. For this reason the two orbitals will differ from one another by more than behavior with respect to a single symmetry plane. These transitions should then be relatively weak as are most $\underline{d} \rightarrow \underline{d}$ transitions.

Based on the correlation of the predicted energies and intensities, with the experimental data, the band assignments listed in Table IV are proposed. We are reasonably confident in the assignments of the two lower energy bands since no other allowed transitions are expected in this region. (The $15e \rightarrow 4a_2$ (2.11 V) and $14a_1 \rightarrow 16e$ (2.39 V) transitions are forbidden in D_{3h} symmetry though allowed in C_{3V}, and the $14a_1 \rightarrow 4a_2$ (2.99 V) transition is dipole forbidden in D_{3h} and C_{3V}). The assignments of the two higher energy bands are much more speculative because the possibility of charge transfer bands has not yet been considered. According to the calculations, the oxygen lone pairs of the terminal alkoxides ($3a_2$, etc.) occur at only slightly lower energies than the metal-metal bonding orbitals $14a_1$ and 15e.

Therefore, oxygen ($p\pi$) to metal charge transfer transitions are also expected to occur in the UV region (e.g. $3a_2 \rightarrow 16e$ at ~2.8 V). Clearly, polarization and/or resonance Raman studies on the absorption bands would be helpful in this regard. A photoelectron spectrum would also be useful in delineating the position of the oxygen lone pairs relative to the metal-metal bonds.

Since the singly-reduced complex is stable in solution, it is interesting to consider what changes in the absorption spectra would be expected upon addition of an electron to the 16e orbital. First, two new low energy transitions would be expected to appear. $16e \rightarrow 4a_2$ (0.60 V) and $16e \rightarrow 17e$ (2.07V). Both of these are allowed in the idealized D_{3h} symmetry, the former being xy polarized and the latter z. Second, since the 16e orbital is now partially occupied, the $15e \rightarrow 16e$ transition might decrease in intensity.

A comparison of the spectra of the normal and reduced species is shown in Figure 4. The reduced complex exhibits a new band at quite low energy ($\leq$0.6 V) which could be assigned to the anticipated $16e \rightarrow 4a_2$ transition. The $15e \rightarrow 16e$ transition at ~1.8 V is observed to lose intensity as expected, and also appears to broaden somewhat. Whether the $16e \rightarrow 17e$ transition is responsible for this broadening or for the increased absorption at ~3V is uncertain. Overall, however, the observed spectral changes are quite consistent with the added electron entering the 16e orbital.

Acknowledgements. We are grateful to the National Science Foundation for financial support at TAMU and the Office of Naval Research for support at I.U.

References and Notes

1. (a) Indiana University. (b) Texas A&M University

2. For extensive references to earlier work both here and elsewhere, see references 1-10 in Ardon, M.; Cotton, F. A.; Dori, Z.; Fang, A.; Kapon, M.; Reisner, G. M.; Shaia, J. Am. Chem. Soc. 1982, 104, 5394.

3. Müller, A.; Jostes, R.; Cotton, F. A. Angew. Chemie, 1980, 92, 921; Intern. Ed. in English, 1980, 19, 875.

4. Bino, A. J. Am. Chem. Soc. 1980, 102, 7990.

5. Bursten, B. E.; Cotton, F. A.; Hall, M. B.; Najjar, R. C. Inorg. Chem., 1982, 21, 302.

6. Cotton, F. A.; Fang, A. J. Am. Chem. Soc. 1982, 104, 113.

7. Fang, A. Ph. D. Dissertation, Texas A&M University, 1982.

8. Chisholm, M. H.; Folting, K.; Huffman, J. C.; Kirkpatrick, C. C. J. Am. Chem. Soc. 1981, 103, 5967.

9. Hall, M. B.; Fenske, R. F. Inorg. Chem., 1972, 11, 768.

10. See the following references for further explanation of the procedure:
(a) Cotton, F. A.; Haas, T. E. Inorg. Chem., 1964, 3, 10.
(b) Bursten, B. E.; Cotton, F. A.; Stanley, G. G. Isr. J. Chem., 1980, 19, 132 (Cf. the Appendix).

Table I. The Molecular Orbitals Formed from 4d Orbitals in the Mo_3^{12+} Cluster

Orbital	Relative Energy (eV)	% Contribution						
		d_{z^2}	$d_{x^2-y^2}$	d_{xy}	d_{xz}	d_{yz}	S	P
$1a_2'$	6.47	--	--	--	84	--	-	16
2e"	3.40	--	--	14	--	83	-	3
3e'	3.30	91	3	--	0	--	2	4
$1a_1"$	2.51	--	--	100	--	--	-	-
2e'	-1.66	2	87	--	8	--	2	1
1e"	-1.97	--	--	85	--	15	-	0
$2a_1'$	-2.45	0	99	--	--	--	1	0
$1a_2"$	-4.57	--	--	--	--	99	-	1
1e'	-5.60	2	8	--	84	--	3	3
$1a_1'$	-7.39	92	0	--	--	--	3	5

Table II. Molecular Orbitals for $Mo_3(\mu_3\text{-}O)(\mu_3\text{-}OH)(\mu_2\text{-}OH)_3(t\text{-}OH')_3(t\text{-}OH'')_3$.[a,b]

Orbital	Relative Energy eV	μ_3-O	μ_3-OH	μ_2-OH	t-OH'	t-OH"	Mo_3	Above 3%
$5a_2$	4.97	0	0	2	5	3	90	87% $1a_2'$
17e	3.41	8	5	0	7	3	77	39% 2e'+34% 3e'
$4a_2$	1.94	0	0	0	8	10	82	82% $1a_1''$
16e	1.34	2	2	6	11	9	70	58% 1e"+10% 2e"
15e	-0.17	2	1	6	12	32	46	36% 1e' + 8% 3e'
$14a_1$	-1.05	38	2	0	10	4	46	30% $1a_1'$+5% $1a_2''$ + 8% $2a_1'$
$3a_2$	-1.44	0	0	0	0	89	12	7% $1a_1''$+5% $1a_2'$
14e	-1.63	21	0	2	3	51	22	10% 1e'+3% 1e"+4% 3e'
$13a_1$	-1.65	15	0	0	1	75	9	4% $1a_1'$
13e	-1.92	3	9	3	1	73	11	
12e	-1.92	1	62	0	25	7	5	
$12a_1$	-2.25	19	0	7	54	9	10	7% $1a_1'$
11e	-2.79	8	2	16	58	3	12	9% 1e"
$2a_2$	-2.85	0	0	0	86	1	13	10% $1a_1''$+3% $1a_2'$
10e	-3.35	30	9	18	8	6	27	8% 1e'+4% 1e"+11% 2e'
$11a_1$	-3.92	0	0	85	7	1	6	5% $2a_1'$
9e	-3.95	5	5	4	59	7	19	8% 1e"+3% 2e'+4% 3e' + 3% 2e"
$1a_2$	-3.95	0	0	90	0	0	10	4% $1a_2'$+6% $2a_2'$
8e	-4.42	2	0	51	12	1	34	25% 1e'+4% 1e"+1% 2e'
$10a_1$	-4.66	13	0	3	25	8	50	42% $1a_1'$+3% $1a_2''$+5% $2a_1'$
7e	-5.27	0	0	71	3	4	21	4% 2e'+7% 3e'+7% 5e'
$9a_1$	-7.47	0	77	1	12	1	9	4% $2a_2''$
$8a_1$	-7.92	2	0	2	5	77	16	4% $1a_2''$+7% $4a_1'$
6e	-8.04	1	0	4	3	73	19	5% 2e'+5% 2e"+6% 4e'
5e	-9.57	0	0	54	23	3	20	7% 1e'+6% 2e"+4% 4e'
$7a_1$	-9.80	1	4	28	42	3	21	10% $1a_2''$+2% $2a_1'$+4% $3a_1'$
4e	-10.03	0	0	26	52	0	20	3% 1e'+3% 2e'+4% 3e'+6% 2e"
$6a_1$	-10.66	0	4	50	24	0	22	5% $1a_1'$+4% $1a_2''$+13% $2a_1'$

[a] t-OH' are on the μ_3-O side; t-OH" are on the μ_3-OH side.

[b] Horizontal broken line separates HOMO (15e) from LUMO (16e).

Table III. Mulliken Populations and Charges.

	Mo_3^{12+}	$Mo_3O_2H^{9+}$	$Mo_3O_5H_4^{6+}$	$Mo_3O_{11}H_{10}$
$1a_1'$	2	1.66	1.76	1.78
1e'	4	3.97	3.65	3.69
$1a_2''$		0.72	0.70	0.70
$2a_1'$		0.84	0.83	0.78
1e"		0.99	1.00	1.41
2e'		0.97	1.10	1.23
$1a_1''$		0.00	0.00	0.35
3e'		0.01	1.28	1.23
2e"		0.31	0.63	1.17
$1a_2'$		0.00	0.16	0.23
Charge on Mo Atom	4.00	2.76	1.74	1.09

Table IV. The Electronic Absorption Spectrum of $Mo_3O(ONe)_{10}$ in Hexane Solution and Suggested Assignments.

OBSERVATIONS			POSSIBLE ASSIGNMENTS			
Maxima nm	eV	ϵ (M^{-1} cm^{-1})	Transition	Polarization	Energy (eV)	Intensity
693	1.79	390	15e → 16e(E'→E")	Z	1.51	Weak
430	2.88	570	15e → 17e(E'→E')	XY	3.58	Weak
287	4.32	25,000	$14a_1$ → 17e(A_1'→E')	XY	4.46	Strong
240	5.17	18,000	15e → $5a_2$(E'→A_2')	XY	5.14	Strong

FIGURE CAPTIONS

Fig. 1. A schematic representation of the type of structure occurring in the $Mo_3(\mu_3\text{-}O)(\mu_3\text{-}OR)(\mu_2\text{-}OR)_3(OR)_6$ compounds.

Fig. 2. Energy levels, calculated in the Fenske-Hall approximation, for the bare Mo_3^{12+} cluster (left), for two intermediate stages of ligand addition, and for the final complete model molecule, $Mo_3(\mu_3\text{-}O)(\mu_3\text{-}OH)$-$(\mu_2\text{-}OH)_3(OH)_6$.

Fig. 3. Contour diagrams for the wave functions of several important molecular orbitals of $Mo_3O(OH)_{10}$. Positive and negative regions are represented by full and broken lines, respectively. Contours begin at 0.005 eA^{-3} and increase by a factor of 2 at each step. For each of the orbitals 15e and 16e, contours are shown in the Mo_3 plane and in a perpendiculr section that contains one Mo-Mo bond. For each of the orbitals $10a_1$ and $14a_1$, there is an in-plane contour and a perpendicular one corresponding to a vertical plane of symmetry.

Fig. 4. Cyclic voltammograms of $Mo_3O(ONe)_{10}$ (V vs. Ag/AgCl): A) Reductive scan in THF. B) Oxidative scan in CH_2Cl_2 showing irreversible oxidation at 0.88 V and product wave at ~-0.5 V.

Fig. 5. Electronic absorption spectra: ——— $Mo_3O(ONe)_{10}$ in hexane, - - $[Mo_3O(ONe)_{10}]^-$ in THF (0.2 M TBAH).

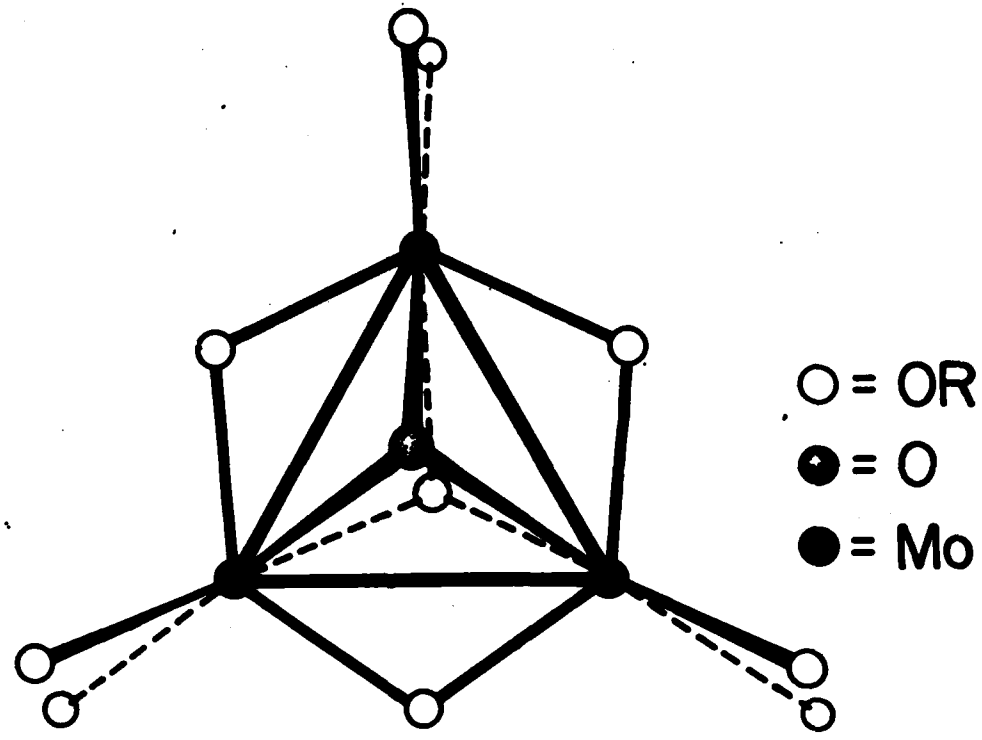
○ = OR
● = O
● = Mo

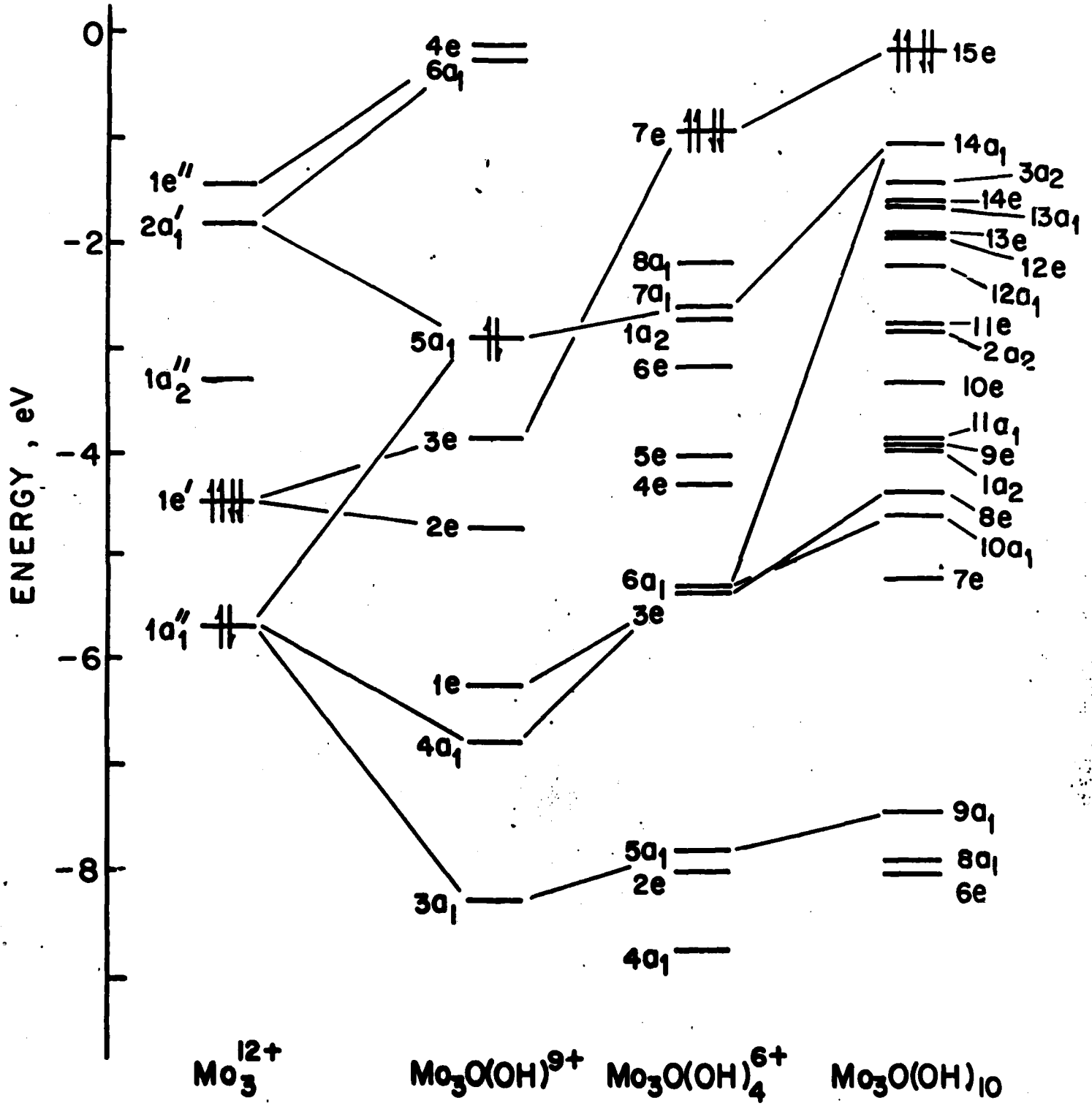
0
-2
-4
-6
-8
ENERGY , eV
1e''
2a'1
1a''2
1e'
1a''1
4e
6a1
5a1
3e
2e
1e
4a1
3a1
7e
8a1
7a1
1a2
6e
5e
4e
6a1
3e
5a1
2e
4a1
15e
14a1
3a2
14e
13a1
13e
12e
12a1
11e
2a2
10e
11a1
9e
1a2
8e
10a1
7e
9a1
8a1
6e
Mo3 12+
Mo3O(OH) 9+
Mo3O(OH)4 6+
Mo3O(OH)10

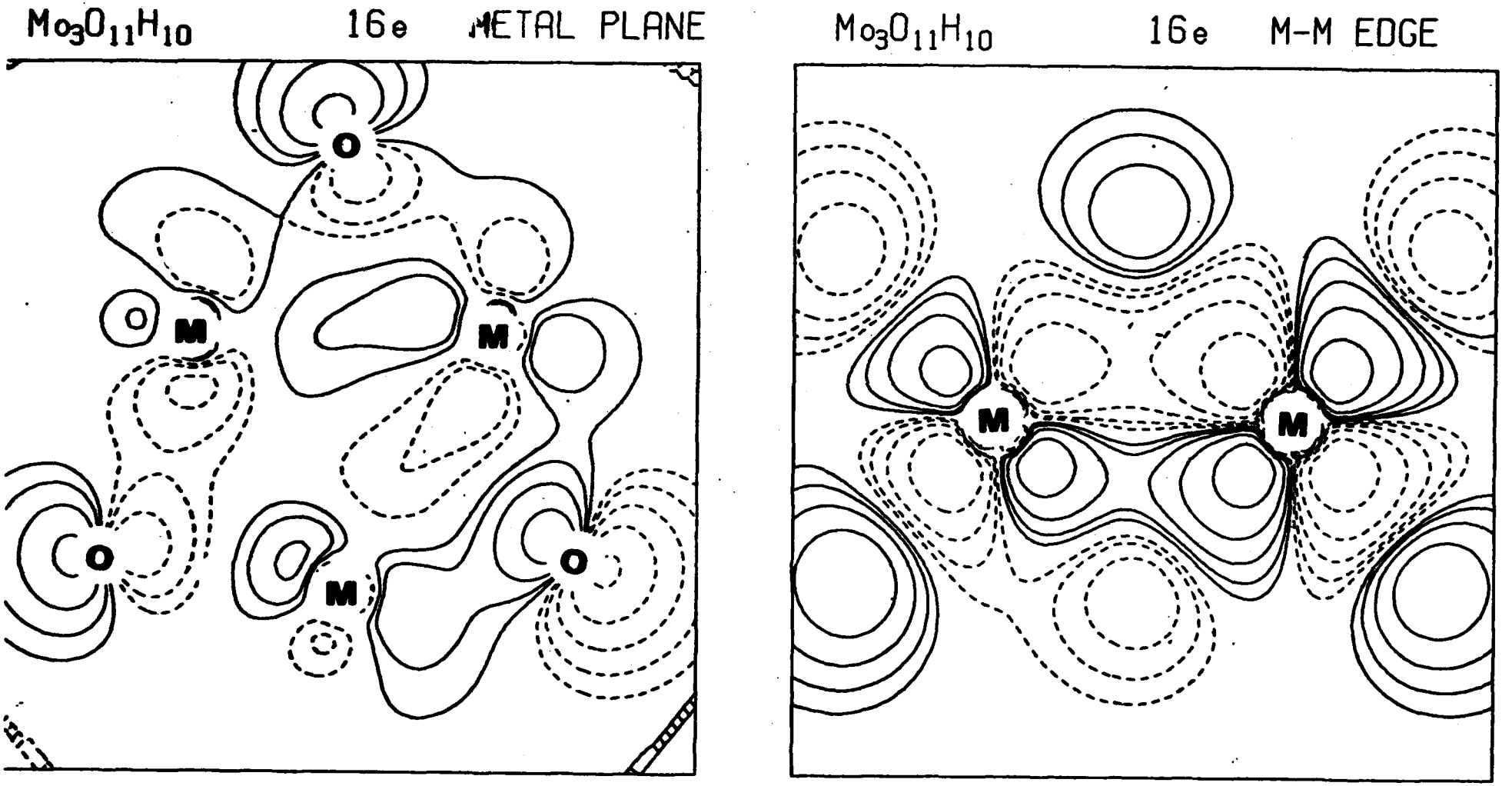
$Mo_3O_{11}H_{10}$ 16e METAL PLANE
O
M
M
O
M
O
$Mo_3O_{11}H_{10}$ 16e M-M EDGE
M
M

$Mo_3O_{11}H_{10}$ 15e METAL PLANE

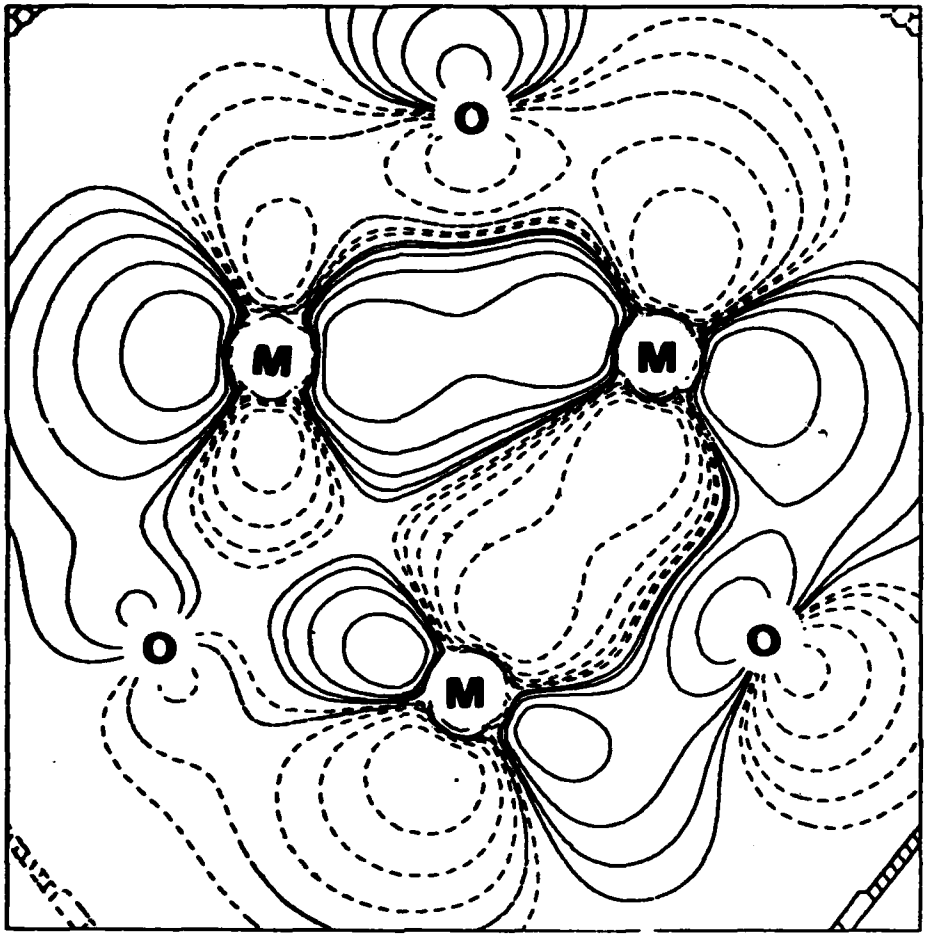

$Mo_3O_{11}H_{10}$ 15e METAL EDGE

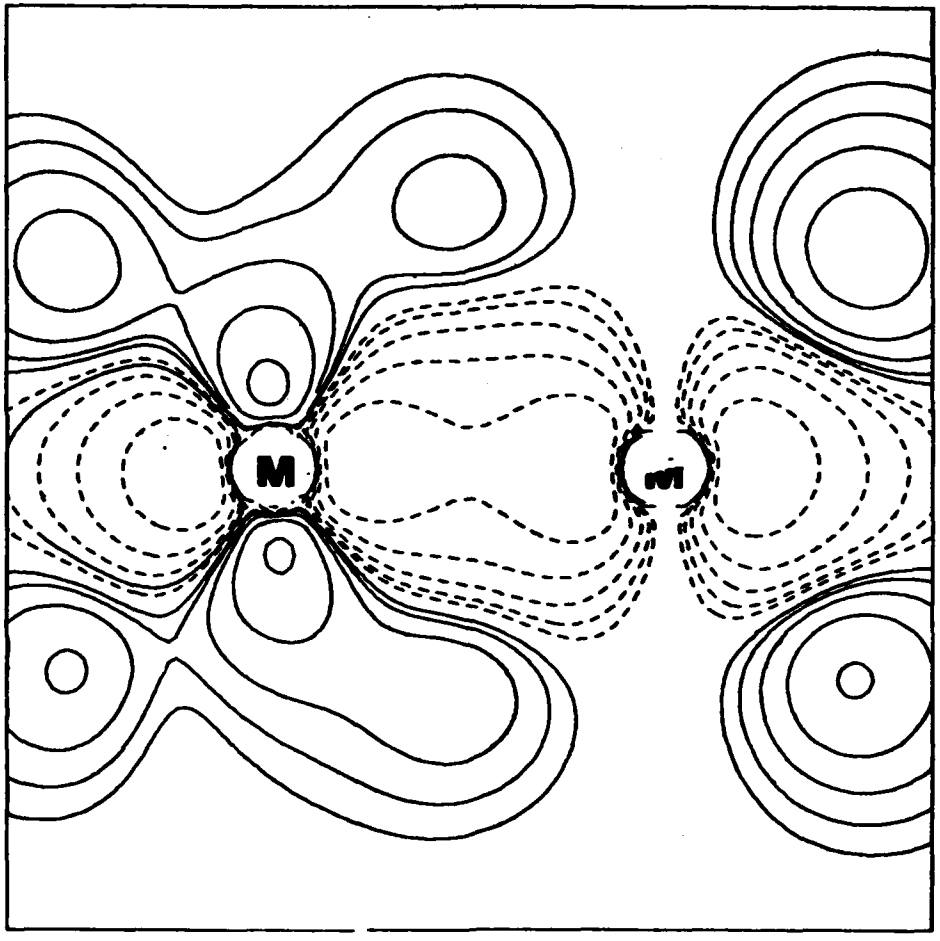

$Mo_3O_{11}H_{10}$ 14A1

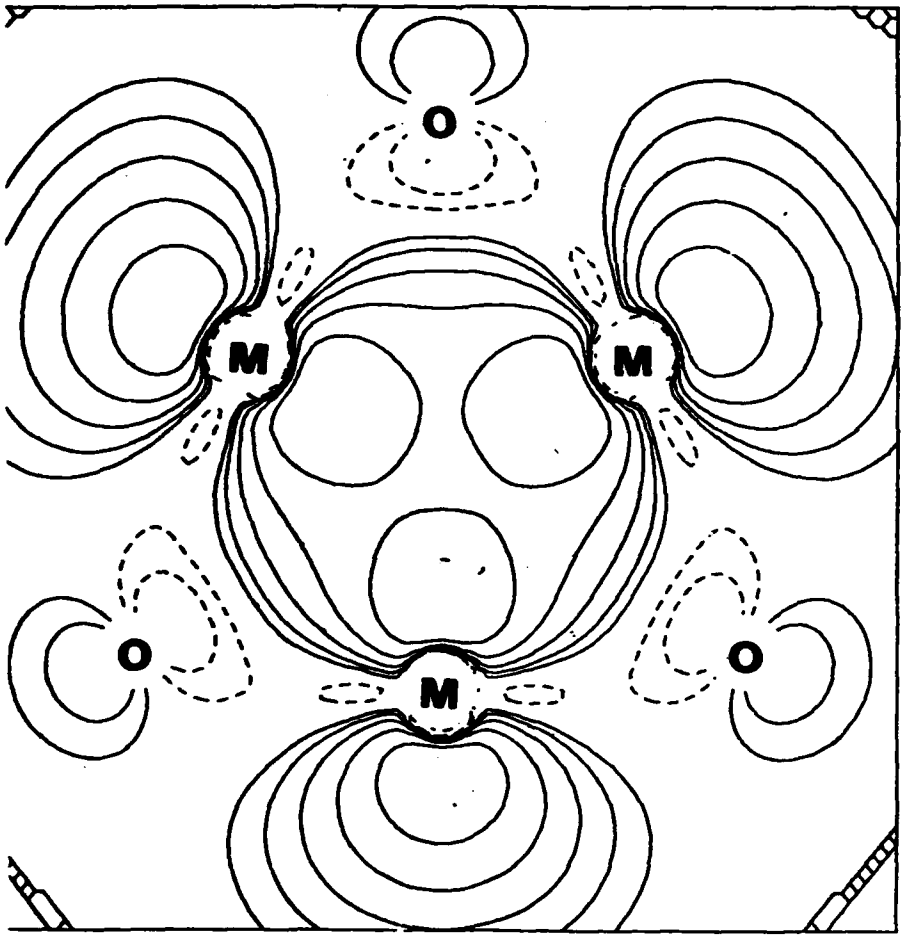

$Mo_3O_{11}H_{10}$ 14A1

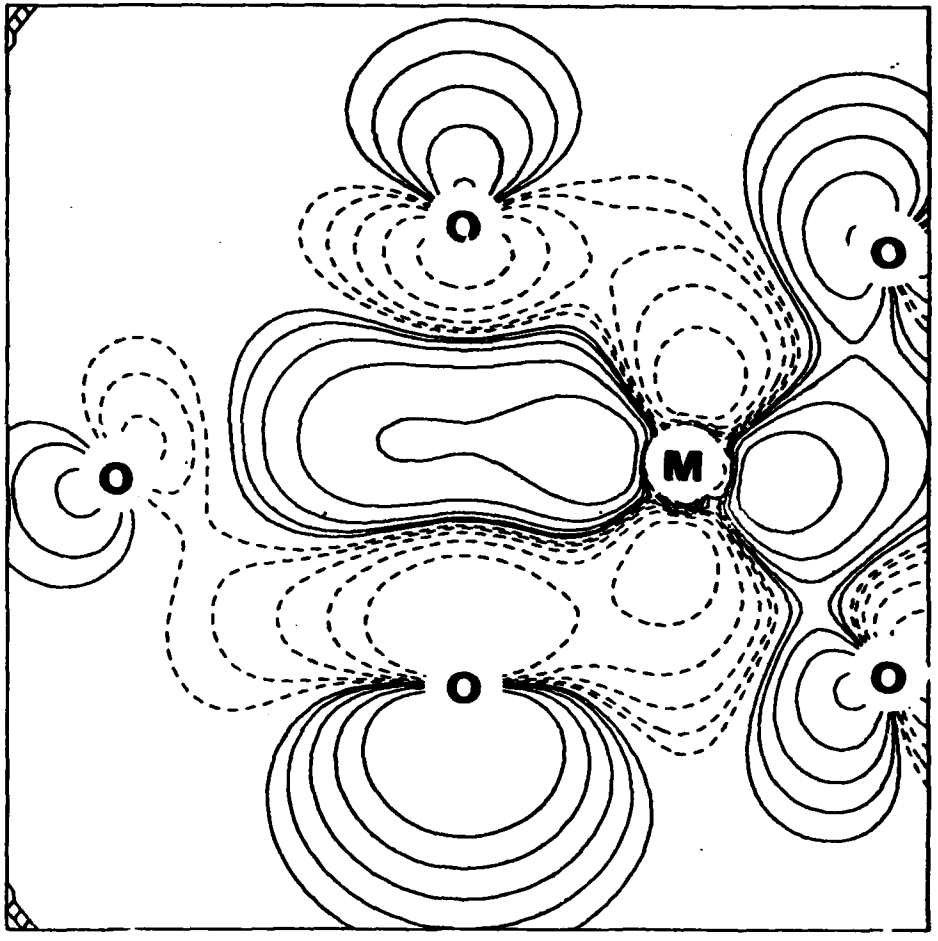

$Mo_3O_{11}H_{10}$ 10A1

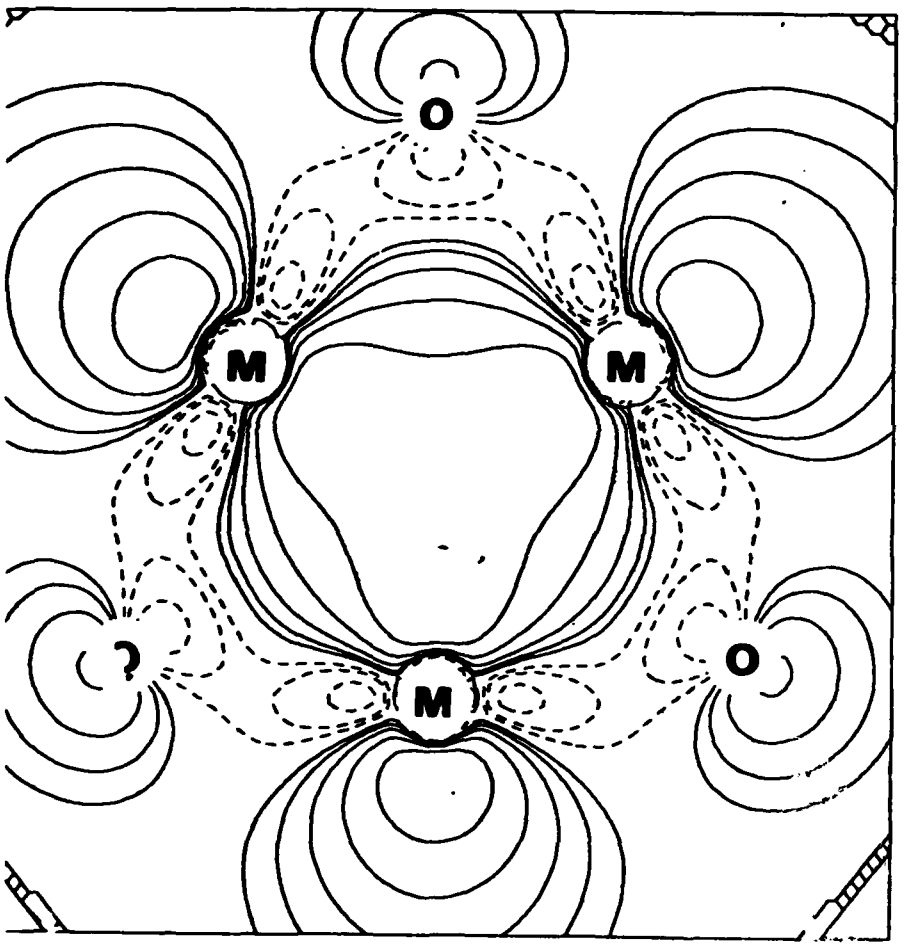

$Mo_3O_{11}H_{10}$ 10A1

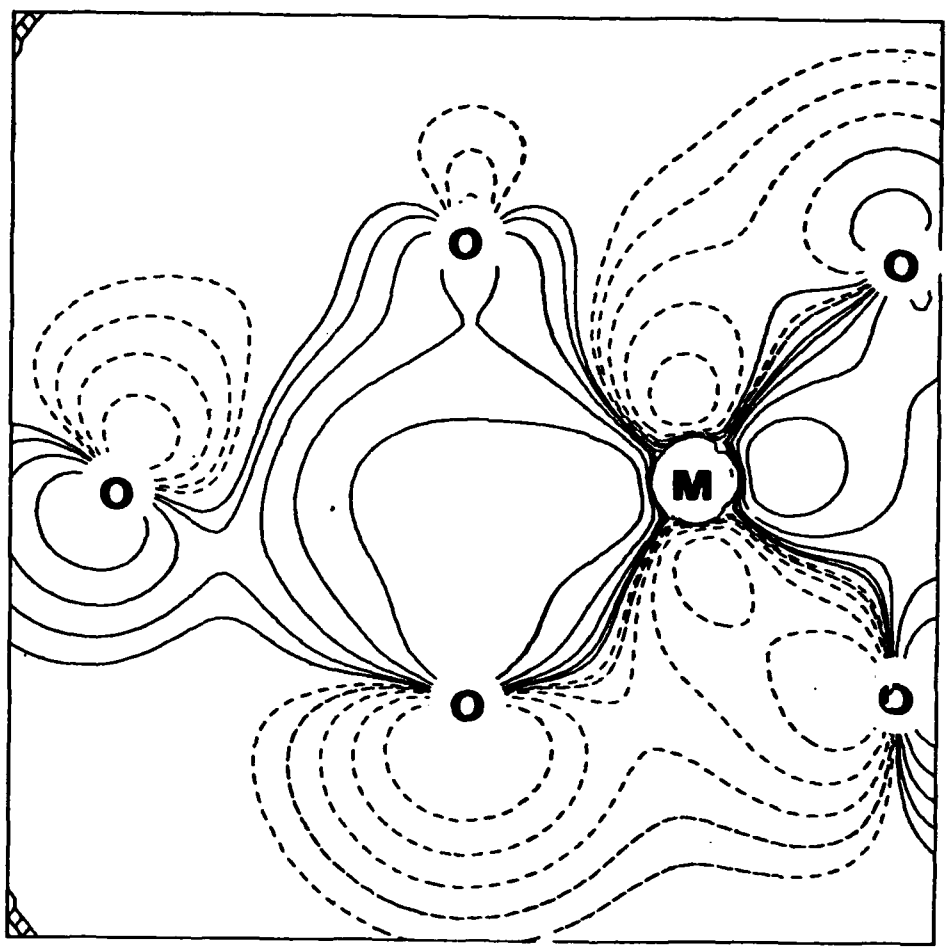

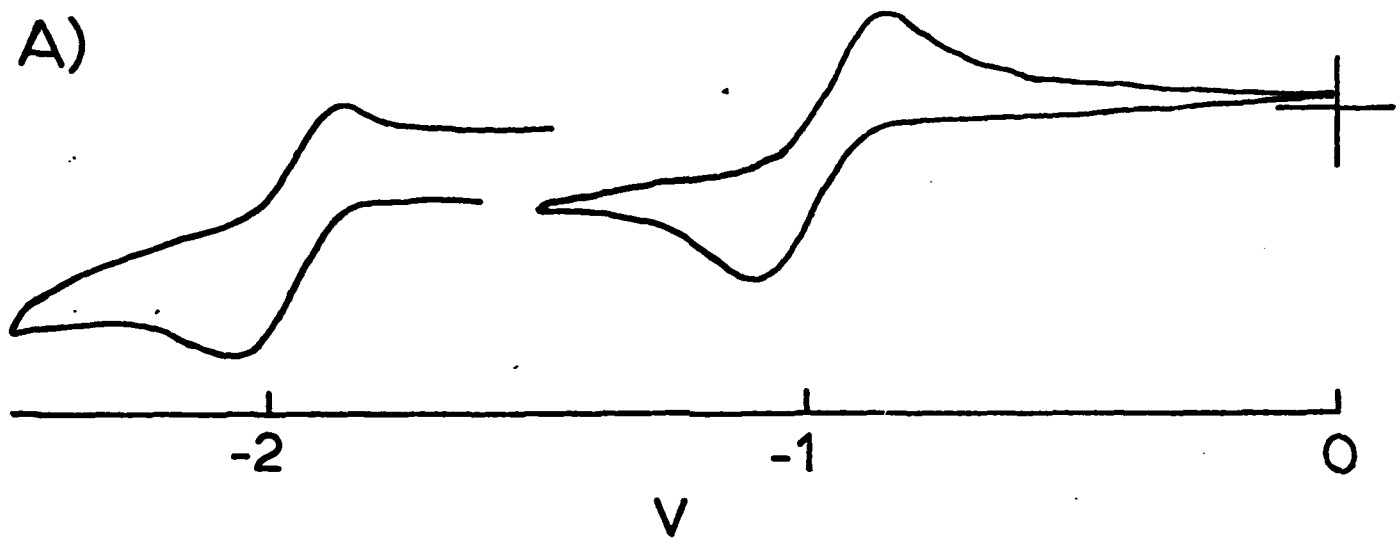
A)
-2
-1
0
V

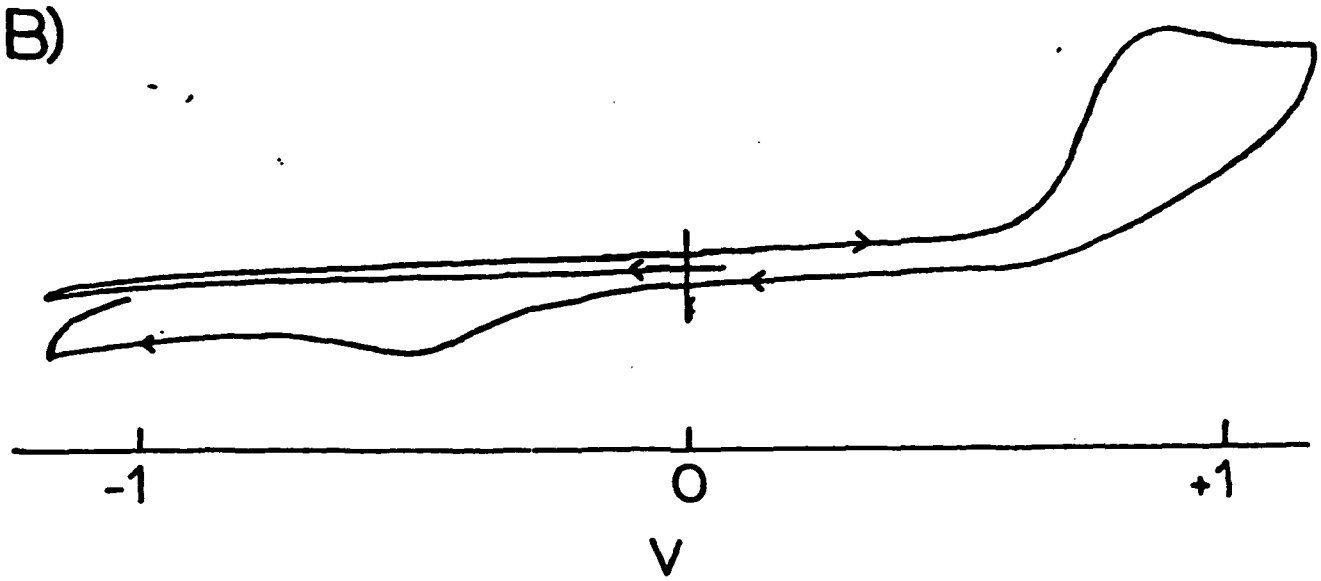
B)
-1
0
+1
V

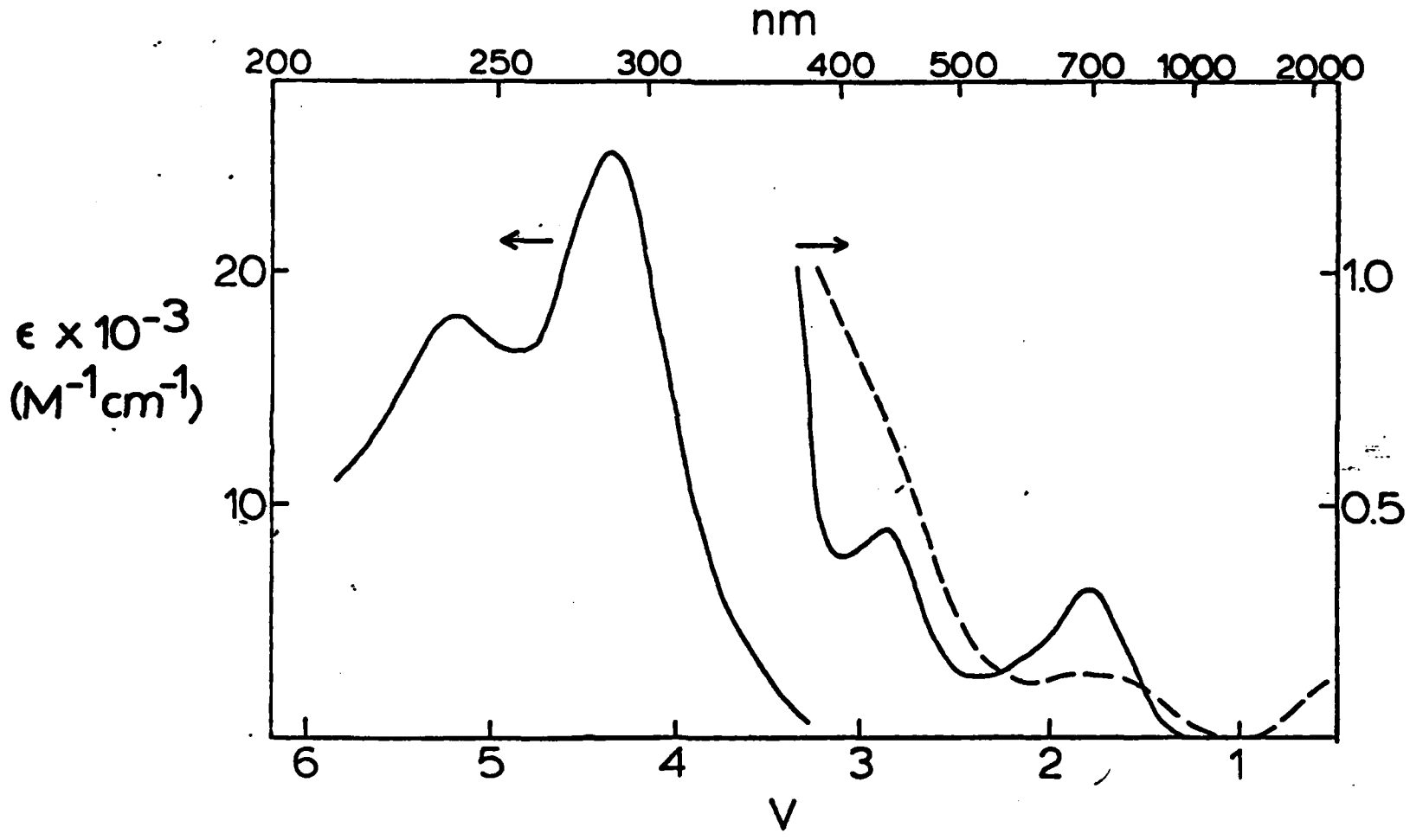
nm
200
250
300
400
500
700
1000
2000
20
10
1.0
0.5
ε x 10⁻³
(M⁻¹cm⁻¹)
6
5
4
3
2
1
V

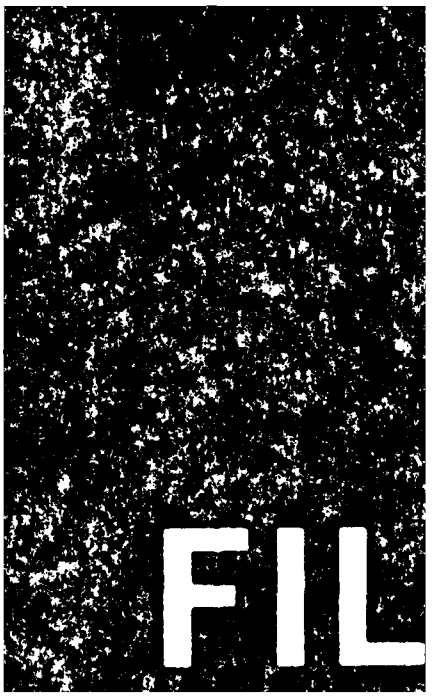
FIL